Journal of Power Sources 187 (2009) 480–486

Contents lists available at ScienceDirect

Journal of Power Sources

journal homepage: www.elsevier.com/locate/jpowsour

$Ln_{0.6}Sr_{0.4}Co_{1-y}Fe_yO_{3-\delta}$ (Ln = La and Nd; y = 0 and 0.5) cathodes with thin yttria-stabilized zirconia electrolytes for intermediate temperature solid oxide fuel cells

Claudia Torres-Garibay*, Desiderio Kovar, Arumugam Manthiram

Electrochemical Energy Laboratory & Materials Science and Engineering Program, The University of Texas at Austin, 1 University Station C2200, Austin, TX 78712, United States

ARTICLE INFO

Article history:
Received 13 September 2008
Received in revised form 4 November 2008
Accepted 5 November 2008
Available online 18 November 2008

Keywords:
Intermediate temperature solid oxide fuel cells
Thin yttria-stabilized zirconia electrolytes
Cobaltite cathodes

ABSTRACT

The electrochemical performances of the solid oxide fuel cells (SOFC) fabricated with $Ln_{0.6}Sr_{0.4}Co_{1-y}Fe_yO_{3-\delta}$ (Ln = La, Nd; y = 0, 0.5) perovskite cathodes, thin yttria-stabilized zirconia (YSZ) electrolytes, and YSZ–Ni anodes by tape casting, co-firing, and screen printing are evaluated at 600–800 °C. Peak power densities of ~550 mW cm^{-2} are achieved at 800 °C with a $La_{0.6}Sr_{0.4}CoO_{3-\delta}$ (LSC) cathode that is known to have high electrical conductivity. Substitution of La by Nd ($Nd_{0.6}Sr_{0.4}CoO_{3-\delta}$) to reduce the thermal expansion coefficient (TEC) results in only a slight decrease in power density despite a lower electrical conductivity. Conversely, substitution of Fe for Co ($La_{0.6}Sr_{0.4}Co_{0.5}Fe_{0.5}O_{3-\delta}$ or $Nd_{0.6}Sr_{0.4}Co_{0.5}Fe_{0.5}O_{3-\delta}$) to reduce the TEC further reduces the cell performance greatly due to a significant decrease in electrical conductivity. However, infiltration of the Fe-substituted cathodes with Ag to increase the electrical conductivity increases the cell performance while preserving the low TEC.

1. Introduction

Solid oxide fuel cells (SOFC) that are able to operate at an intermediate temperature of 600–800 °C offer significant advantages over conventional SOFCs operating at higher temperatures [1–4]. For example, the overall cost could be decreased if interconnects, heat exchangers, and structural components could be fabricated with inexpensive metals. Lower operating temperatures would also enhance the durability of SOFC by minimizing thermal stresses experienced by the components during temperature cycling. However, the major issues with decreasing the operating temperature are the performance losses arising from lower electrolyte conductivity and inadequate catalytic activity at the cathode for the oxygen reduction reaction. While the electrolyte conductivity issue can be addressed by reducing the thickness of the electrolyte using established, inexpensive technologies like tape casting, development of more efficient cathodes is needed to overcome the poor oxygen reduction kinetics.

Although $La_{1-x}Sr_xMnO_{3-\delta}$ (LSM) is commonly used as a cathode in high temperature SOFC [5–8], it cannot be used for intermediate temperature solid oxide fuel cells (IT-SOFC) operating at <900 °C as the activation polarization of LSM increases considerably with decreasing temperature [9]. In this regard, $La_{1-x}Sr_xCoO_{3-\delta}$ is appealing as it exhibits high catalytic activity at intermediate temperatures [10,11]. However, $La_{1-x}Sr_xCoO_{3-\delta}$ exhibits a high thermal expansion coefficient (TEC) due to the low spin to high spin transition associated with the Co^{3+} ions [12], which is undesirable as it can lead to large thermal expansion mismatch with other cell components. A tradeoff between catalytic activity and TEC has been achieved by partially substituting Co by Fe in $La_{1-x}Sr_xCo_{1-y}Fe_yO_{3-\delta}$ [12] or by replacing La^{3+} by smaller lanthanide ions like Nd^{3+} [13–15]. The less ionic Nd–O bonds compared to the more ionic La–O bonds decreases the TEC, and optimized compositions like $Nd_{0.6}Sr_{0.4}CoO_{3-\delta}$ exhibit good performance [16]. Also, substitution of Co by Fe in $Nd_{0.6}Sr_{0.4}Co_{1-y}Fe_yO_{3-\delta}$ reduces the TEC further [17]. Because the substitution of Fe for Co lowers the electrical conductivity and catalytic activity, impregnation of $Nd_{0.6}Sr_{0.4}Co_{0.5}Fe_{0.5}O_3$ with silver has been attempted to enhance the electrical conductivity and catalytic activity [18].

However, most of these studies have been carried out employing relatively thick $La_{0.8}Sr_{0.2}Ga_{0.8}Mg_{0.2}O_{3-\delta}$ (LSGM) electrolyte. Since the ohmic polarization occurring with thick electrolytes could dominate at moderate to high current densities, we investigate here the electrochemical performances of the $Nd_{0.6}Sr_{0.4}Co_{1-y}Fe_yO_{3-\delta}$ cathodes with thin (<15 μm) yttria-stabilized zirconia (YSZ) electrolytes at 600–800 °C. The cells are manufactured by tape casting, co-firing, and screen printing

* Corresponding author. Present address: Materials Science and Engineering Department, University of Michigan, 2300 Hayward St., Ann Arbor, MI 48109, USA Tel.: +1 734 223 0359; fax: +1 734 763 4788.
E-mail addresses: clautoga@alumni.utexas.net (C. Torres-Garibay), dkovar@mail.utexas.edu (D. Kovar), rmanth@mail.utexas.edu (A. Manthiram).

0378-7753/$ – see front matter © 2008 Elsevier B.V. All rights reserved.
doi:10.1016/j.jpowsour.2008.11.025

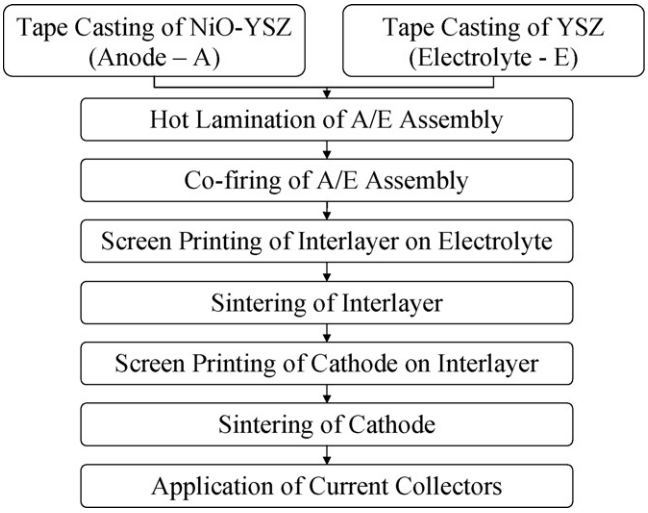

Fig. 1. Manufacturing process for producing the SOFC electrolyte–electrode assembly.

with $Nd_{0.6}Sr_{0.4}CoO_{3-\delta}$ (NSC), $Nd_{0.6}Sr_{0.4}Co_{0.5}Fe_{0.5}O_{3-\delta}$ (NSCF), and silver-impregnated $Nd_{0.6}Sr_{0.4}Co_{0.5}Fe_{0.5-\delta}$ (NSCF–Ag) cathodes. For a comparison, the data collected with the $La_{0.6}Sr_{0.4}CoO_{3-\delta}$ (LSC) and $La_{0.6}Sr_{0.4}Co_{0.5}Fe_{0.5}O_{3-\delta}$ (LSCF) cathodes are also presented.

2. Experimental

2.1. Cathode materials preparation

LSC and NSC were synthesized by solid state reactions. The starting materials were La_2O_3 (Alfa Aesar) (for LSC), Nd_2O_3 (Alfa Aesar) (for NSC), $SrCO_3$ (Alfa Aesar) and Co_3O_4 (GFS Chemicals). The lanthanide oxides were dried for 2 h at 1000 °C and weighed immediately after drying. Required amounts of the reactants were ground in an agate mortar and pestle, fired in air for 48 h (LSC) or 72 h (NSC), with an intermediate grinding every 24 h. Finally, the powders were ball-milled dry and ground by hand in ethanol to achieve the desired particle size. LSCF and NSCF were synthesized by a co-precipitation method, employing La_2O_3 (Alfa Aesar), Nd_2O_3 (Alfa Aesar), $SrCO_3$ (Alfa Aesar), $Co(CH_3COO)_2{\cdot}H_2O$ (Spectrum), and $Fe(CH_3COO)_2$ (GFS Chemicals) as starting materials. Required amounts of the raw materials were dissolved in dilute nitric acid and a 10% (w/v) solution containing equal amounts of KOH and K_2CO_3 was added slowly until the pH raised above 11 to co-precipitate the metal ions as carbonates and hydroxides. The co-precipitate was filtered, washed with deionized water several times, dried overnight in an air-oven, calcined in air at 500 °C for 5 h, ground by hand, and fired in air for 24 h at 1200 °C. The products were then dry ball milled or hand ground in ethanol to achieve the desired particle size distribution.

2.2. Manufacturing of the electrolyte–electrode assembly

Fig. 1 shows a schematic of the manufacturing process employed to produce the SOFC electrolyte–electrode assembly. The electrolyte was prepared with 8 mol% Y_2O_3-doped zirconia (YSZ, Tosoh) and the anode was prepared from a mixture of 54 vol% NiO (J.T. Baker) and 46 vol% YSZ (8 mol% Y_2O_3-doped zirconia, Tosoh). The electrolyte powders were dispersed with a surfactant in an organic solvent by ball milling for 12 h. The anode powders were dispersed with a surfactant in a mixture of solvents by ball milling for 24 h. Binders and plasticizers were then added to each suspension, followed by ball milling for 24 h. Specific details about materials and ratios used in the formulations are given in Tables 1 and 2. The slurries were then tape cast separately onto a glass substrate using a doctor blade with a gap of 100 μm for the electrolyte and 400 μm for the anode. After drying, discs with a diameter of 22.2 mm were punched from the anode and electrolyte tapes. Six discs of the anode material and one disc of electrolyte material were stacked, and placed between 6.35 mm thick polycarbonate plates that were covered with a non-stick coated aluminum foil (All-Foils, Inc.). The stacks were then hot laminated for 10 min at 85 °C and 19.3 MPa to produce the anode–electrolyte assembly.

Table 1
Electrolyte slurry composition [21].

Component	Function	ρ (g/cc)	Wt.%	Vol.%
8-YSZ (Tosoh)	Ceramic powder	5.9	45.0	10.4
Ethyl alcohol	Solvent	0.79	22.2	38.5
Methyl ethyl ketone	Solvent	0.8	22.2	38.0
Phosphate ester	Dispersant	1.05	0.7	0.9
Polyvinyl butyral (Butvar B98)	Binder	1.1	4.2	5.2
Polyethylene glycol	Plasticizer	1.1	4.6	5.7
Benzyl butyl phthalate	Plasticizer	1.12	1.1	1.3

Following lamination, the organics were pyrolyzed by heating at 20 °C h^{-1} from room temperature to 160 °C, followed by heating at 40 °C h^{-1} to 400 °C, 100 °C h^{-1} to 500 °C, and cooling at 2 °C min^{-1}. After the binder removal, the anode/electrolyte assembly was co-fired for 2 h at 1400 °C with heating and cooling rates of 2 °C min^{-1}. To maintain the flatness of the assemblies during pyrolysis and firing, they were covered with graphite and placed with the anode side facing up between flat layers of coarse YSZ inside of an alumina crucible. An alumina plate with an additional mass was placed on top to produce a compressive pressure of about 500 Pa on each assembly.

After co-firing of the anode/electrolyte assembly, a $Ce_{0.9}Gd_{0.1}O_{2-\delta}$ (GDC) interlayer was applied to the electrolyte prior to screen printing of the cathode. GDC powder was prepared using a glycine nitrate combustion synthesis technique [19]. Pastes for screen printing the interlayer and the cathode materials were prepared by mixing the oxide powders with an organic vehicle (W. C. Heraeus, V-006) in a 1:1 weight ratio of the oxide to the organic vehicle for the interlayer paste and 3:2 weight ratio for the cathode paste. After screen printing the interlayer, the interlayer/anode/electrolyte assembly was fired for 2 h at 1300 °C. Cathodes were then applied onto the sintered interlayer by screen printing in three passes. The cathode/interlayer/electrolyte/anode assemblies were fired for 2 h at a temperature determined by reactivity tests. Reactivity tests were conducted by firing a 1:1 (w/w) mixture of GDC and the cathode material and then examining them by XRD to determine if reactions had occurred between the GDC and the cathode. The firing temperature subsequently used for the cathode/interlayer/electrolyte/anode assembly was the maximum temperature at which no reaction occurred between the cathode and GDC. These temperatures were 1100 °C for LSC and LSCF and 1200 °C for NSC and NSCF-based cells. A limited number of cells were fired at lower temperatures to determine the influence of cathode firing temperature on cell performance.

Table 2
Anode slurry composition (adapted from Mistler [22]).

Component	Function	ρ (g/cc)	Wt.%	Vol%
NiO (Baker)	Ceramic powder	6.67	35.4	9.6
8-YSZ (Tosoh)	Ceramic powder	5.9	26.6	8.2
Ethyl alcohol	Solvent	0.79	12.3	28.3
Toluene	Solvent	0.805	18.4	41.5
Phosphate ester	Dispersant	1.05	1.2	2.5
Polyvinyl butyral (Butvar B79)	Binder	1.083	3.1	5.2
Benzyl butyl phthalate	Plasticizer	1.12	3.1	5.0

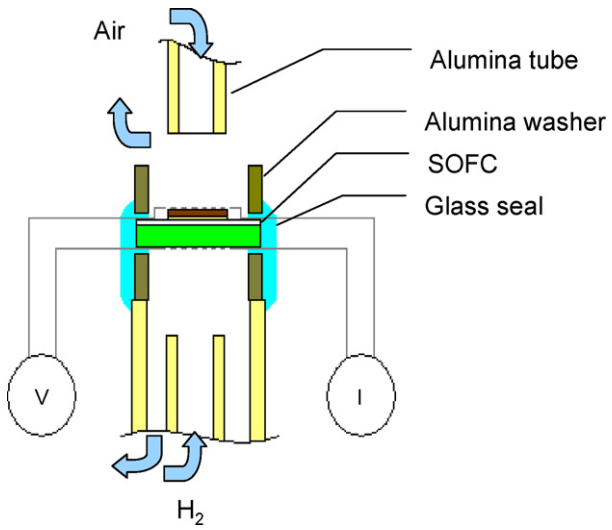

Fig. 2. Schematic of the SOFC test set-up.

2.3. Electrolyte–electrode assembly with silver-impregnated NSCF (NSCF–Ag) cathodes

The electrolyte–electrode assemblies were prepared with NSCF cathodes that were loaded with 0.1 mg cm^{-2} (~0.5 wt.%) of Ag by impregnation. A solution of $AgNO_3$ (Alfa Aesar, ACS 99.9+ %) in a 1:1 (v/v) mixture of ethanol and water was used. A 0.2 M solution was used to impregnate ~1 mg cathodes using a micropipette by successive infiltrations of small amounts of the solution. The fraction of silver impregnated into the cathode was calculated based on the difference in the masses of the cathode before and after infiltration. Nitrate was removed by firing the assembly at 700 °C for 3 h.

2.4. Electrochemical evaluation

Prior to electrochemical testing, platinum current collectors were attached to the electrodes. The current collector consisted of a 5 mm^2 platinum gauze interwoven and welded with a 0.127 mm diameter platinum wire. A small amount of platinum ink (Heraeus, CL11-5100) was applied to the border of the gauze before it was placed on the electrode. After application of the current collectors, the cells were fired at 900 °C for 30 min to remove the organics in the platinum ink and to sinter the platinum and, in the case of NSCF–Ag, the silver particles.

A schematic of the test set-up is shown in Fig. 2. The cell was attached to two alumina rings using a glass paste made with 95 wt.% glass powder having a high TEC (Specialty Glass, SP737 TF-200) and 5 wt.% adhesive (Duco Cement). The glass paste was prepared by mixing the glass powder and adhesive with acetone until a homogeneous consistency was achieved. The alumina rings were then placed in contact with the cells and were attached to the alumina tubes with a small amount of adhesive. Electrical connections were made through the glass paste that was applied surrounding the alumina rings and the top section of the tube, as shown in Fig. 2.

The set-up was heated at 2 °C min^{-1} until it reached 875 °C, which is slightly above the softening point of the glass, held at 875 °C for 2 h, and then decreased at 2 °C min^{-1} to the first operating temperature of 800 °C. After at least 2 h of flowing 100 sccm of N_2 to the anode side, and if no leaks were found, N_2 was slowly replaced with humidified H_2 (~3% H_2O at 30 °C). The introduction of H_2 resulted in the reduction of NiO to Ni within the anode. Air was gradually supplied to the cathode until the flux reached 100 sccm. Once the open circuit voltage (OCV) had stabilized at its maximum value, the electrochemical tests were initiated, first at 800 °C, then at 700 °C, and lastly at 600 °C. The tests were then repeated at the same temperatures but in an ascending order. *I–V* measurements were performed with a fuel cell test station, and at least two tests for each cathode composition were performed at each temperature.

Table 3
Maximum power densities (W cm^{-2}) obtained at operating temperatures of 600–800 °C for cells fabricated with various perovskites cathodes.

Cathode	800 °C	700 °C	600 °C
LSC1000	0.549	0.232	0.069
LSC1100	0.344	0.148	0.049
LSCF1000	0.378	0.159	0.045
LSCF1100	0.274	0.120	0.040
NSC1100	0.404	0.192	0.065
NSCF1200	0.173	0.066	0.021
NSCF–Ag1200	0.213	0.083	0.023

3. Results

The average maximum power density values measured for each composition at various operating temperatures are given in Table 3. The number displayed after the cathode designation is the cathode sintering temperature. *I–V* traces and power densities for cells with the LSC cathodes that were fired at 1000 °C are shown in Fig. 3a. Peak power density is over 0.5 W cm^{-2} at an operating temperature of 800 °C. As expected, the power densities drop with operating temperatures to 0.2 W cm^{-2} at 700 °C, and to 0.07 W cm^{-2} at 600 °C. *I–V* plots and power densities for cells with LSC cathodes fired at 1100 °C are shown in Fig. 3b. Compared to the cells with cathodes fired at 1000 °C, the cells with cathodes fired at 1100 °C exhibit a more pronounced voltage drop at lower current densities. For example, at an operating temperature of 800 °C, cells with cathodes fired

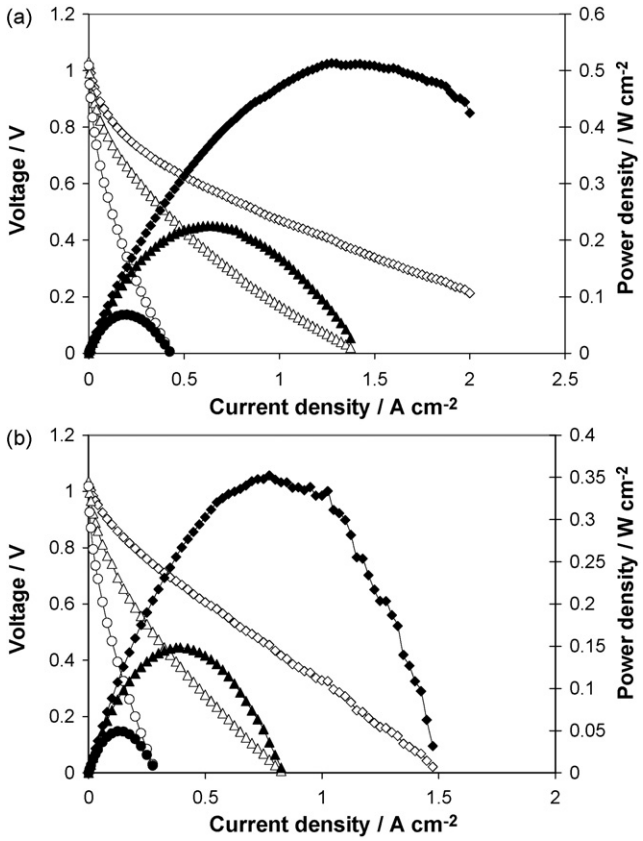

Fig. 3. *I–V* curves (open symbols) and power densities (closed symbols) for the cells fabricated with (a) LSC cathodes fired at 1000 °C and (b) LSC cathodes fired at 1100 °C.

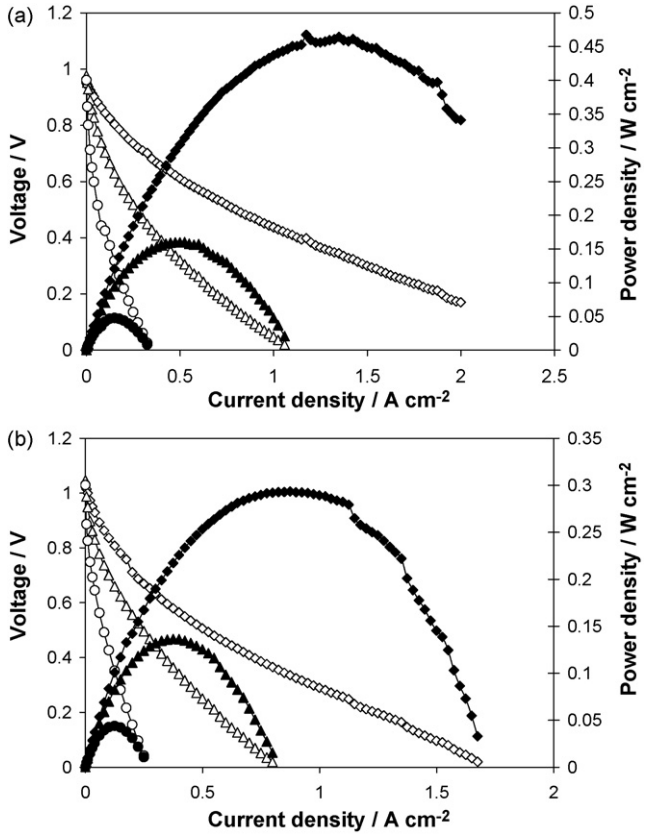

Fig. 4. *I–V* curves (open symbols) and power densities (closed symbols) for the cells fabricated with (a) LSCF cathodes fired at 1000 °C and (b) LSCF cathodes fired at 1100 °C.

at 1100 °C exhibit a power density 37% lower than the cells with similar cathodes fired at 1000 °C. Similar trends are observed at operating temperatures of 700 °C and 600 °C.

I–V curves and power densities collected with the LSCF cathodes fired at 1000 °C and 1100 °C are shown, respectively, in Fig. 4a and b. Compared to the cells with LSC cathodes, the cells with the LSCF cathodes exhibit lower power densities. For example, the maximum power density for the cell with a LSCF cathode fired at 1000 °C (Fig. 4a) is about 31% lower than that for the cell with a LSC cathode fired at the same temperature (Fig. 3a). Comparing the LSCF-based cells with a cathode firing temperature of 1000 °C (Fig. 4a) and 1100 °C (Fig. 4b), it is apparent that the higher cathode firing temperature results in a reduction in the power density at all of the operating temperatures that were investigated. For example, at an operating temperature of 800 °C, the peak power density for the cell with the LSCF cathode fired at 1000 °C is 28% higher than that for the cell with the LSCF cathode fired at 1100 °C. It is clear that firing temperatures above 1000 °C for both the LSC and LSCF cathodes result in reduced cell performance.

I–V measurements and power densities for the cells with the NSC and NSCF cathodes are presented in Fig. 5a and b. Comparing the performance of the cells with the NSC cathodes to those with the LSC cathodes (Fig. 3a), both fired at 1100 °C, we see that the performance with the NSC cathodes is slightly better than that with the LSC cathodes. Cells with the NSCF cathodes fired at 1200 °C have slightly lower power densities than the cells with the LSCF cathodes fired at 1100 °C, but at least some of this difference may result from differences in the cathode firing temperature. Thus, the substitution of Nd by La does not have a significant effect on the cell performance at intermediate temperatures.

Fig. 5c shows the *I–V* plots and power density curves for the cells with the NSCF cathodes that were infiltrated with Ag. Comparing

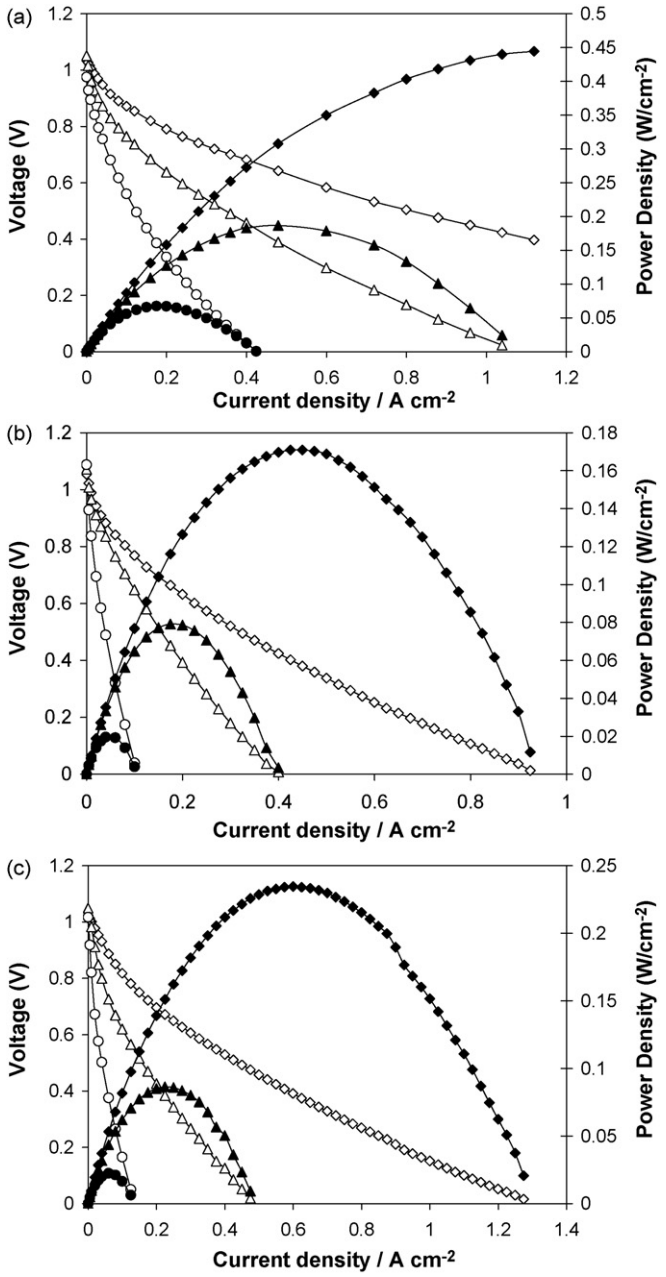

Fig. 5. *I–V* curves (open symbols) and power densities (closed symbols) for the cells fabricated with (a) NSC cathodes (b) NSCF cathodes, and (c) NSCF–Ag cathodes.

Fig. 5c to Fig. 5b, it is apparent that the power density increases due to the presence of the conductive Ag in the cathode. For example, at an operating temperature of 800 °C, the peak power density for the NSCF–Ag-based cell is about 19% higher than that for the NSCF-based cell.

4. Discussion

4.1. Influence of cathode sintering temperature for LSC and LSCF

Table 3 provides a summary of the cell testing data. Since all the cells are identical except for the cathodes, it is clear that the differences in performance (catalytic activity) could result from the differences in the properties of the cathode materials such as electrical conductivity, oxide ion conductivity, and surface exchange properties. There are several microstructural factors that could

influence both these parameters and consequently the catalytic activity and cell performance. For example, increasing the sintering temperature could result in a reduction in the total porosity of the cathode due to densification. Densification will increase the electrical conductivity of the cathode and thus, should improve cell performance at moderate current densities where performance is mostly limited by activation and ohmic polarizations. However, the decrease in porosity would also lead to an increase in concentration polarization because of reduced gas flow through the cathode and therefore a reduction in power density might occur at high current densities. Conversely, higher sintering temperatures could instead result in particle/pore coarsening rather than densification. Coarsening would decrease the total number of reaction sites available for the oxygen reduction reaction and therefore result in increased activation polarization at low current densities, but have little effect at higher current densities since coarsening does not change the total porosity. Thus, a comparison of the *I–V* curves at low and high current densities should help to determine how changes in cathode sintering temperatures influence the microstructure and the cell performance.

Fig. 6 shows the initial portions of *I–V* traces at 800 °C, 700 °C, and 600 °C. The voltage values are averages of the results of the two tests carried out for each cathode composition. Note that differences in OCV could result from the differences in oxygen pressures between the cathode and the anode sides of the cell. Such differences reflect the quality of the glass seal, which is affected by deviations in the flatness of the cell, glass paste composition, and application method. Although not related to the intrinsic material properties of the cell, the OCV can affect the measured maximum power density. Thus, rather than comparing OCV or power densities, it is more instructive to focus on the slope of the initial portion of the *I–V* traces, which is directly related to differences in material properties.

From Fig. 6, it can be seen that the *I–V* traces for LSC and LSCF-based cells have a steeper initial slope when the cathode sintering temperature is increased. This decrease in performance with increasing sintering temperature at low current densities is consistent with increased activation polarization due to particle coarsening and a concomitant decrease in the number of reaction sites that are available in the cathode. Although densification could also occur to offset some of the loss in performance due to the reduction in the number of reaction sites, the observed differences in slope suggest that the performance of these cells is dominated by particle coarsening rather than densification. Secondary electron (SE) micrographs of the cross-section of the cells in Fig. 7a and b for the LSC-based cells and Fig. 8a and b for the LSCF-based cells show that cathodes sintered at high temperatures exhibit increased particle and pore sizes, which confirms that coarsening rather than densification dominates at these cathode sintering temperatures.

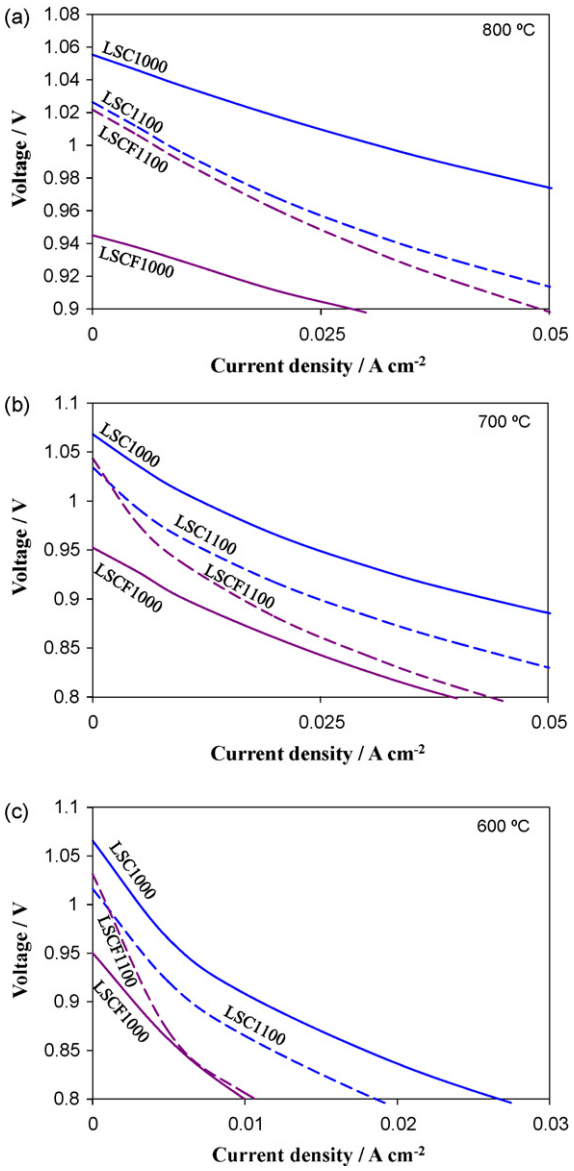

Fig. 6. Comparison of average *I–V* traces at low current densities for the cells fabricated with LSC and LSCF cathodes operating at (a) 800 °C (b) 700 °C, and (c) 600 °C. The number after the cathode composition refers to cathode firing temperature.

4.2. Comparison of the NSC- and LSC-based cells

Contrary to expectations, substitution of La^{3+} by Nd^{3+} in the cathode was found to improve the performance of the cells even though the electrical conductivity and electrocatalytic activity for the oxygen reduction reaction are known to be higher for LSC than for NSC [15]. Because the electrical conductivity of LSC is almost two times higher than that of NSC (2238 S cm^{-1} vs. 1257 S cm^{-1} at 800 °C) [15,17] it is likely that the differences in the sintering characteristics of the two cathodes play a critical role on the overall catalytic activity and cell performance. Since the performance of the cell with NSC cathode is similar to that with the LSC cathode, the NSC cathode with a lower TEC is attractive compared to the LSC cathodes for intermediate temperature SOFC.

4.3. Comparison of the LSC- and LSCF-based cells and NSC- and NSCF-based cells

Fig. 9a and b shows the micrographs of the fracture surfaces of the cells with the NSC and NSCF cathodes. The decrease in the performance of the cells with the Fe-doped cathodes is expected since the substitution of Co for Fe causes a decrease in the electrical conductivity. For example, the electrical conductivity of LSC is 2238 S cm^{-1} at 800 °C, while that of LSCF (with 80% substitution of Co by Fe) is only 333 S cm^{-1} [12]; NSC exhibits a conductivity of 1257 S cm^{-1}, but it drops to 363 S cm^{-1} on doping when doped with Fe (NSCF) [17].

I–V plots for all the cells (Figs. 3–6) have a positive curvature, except at very high current densities. The magnitude of the slope of the traces at very low current densities is related to the area specific resistance of the cell. This resistance includes the ohmic resistance of the electrolyte and the effective charge transfer resistance of the cathode. Given the thicknesses of the electrolyte and

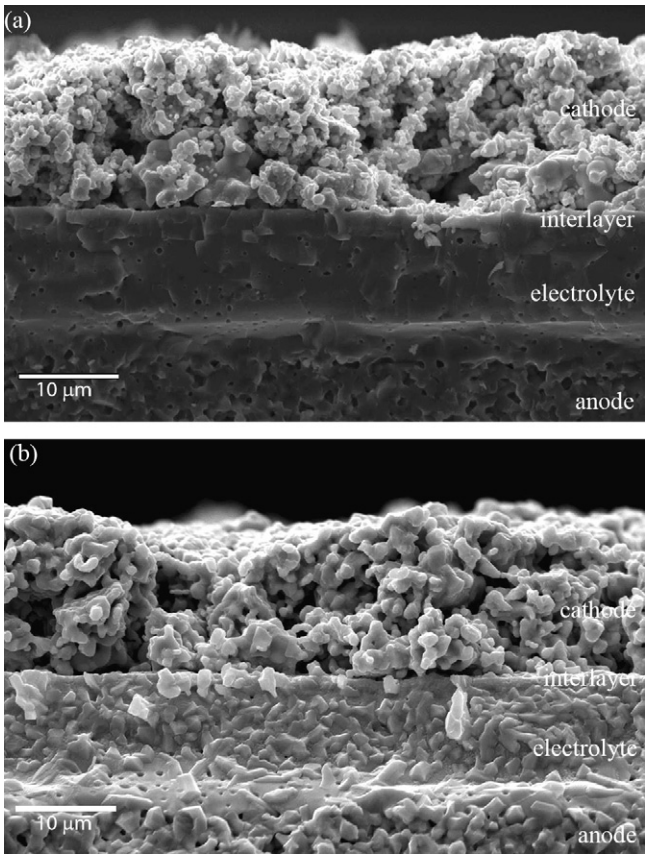

Fig. 7. SEM of the cells with the LSC cathodes fired at (a) 1000 °C and (b) 1100 °C.

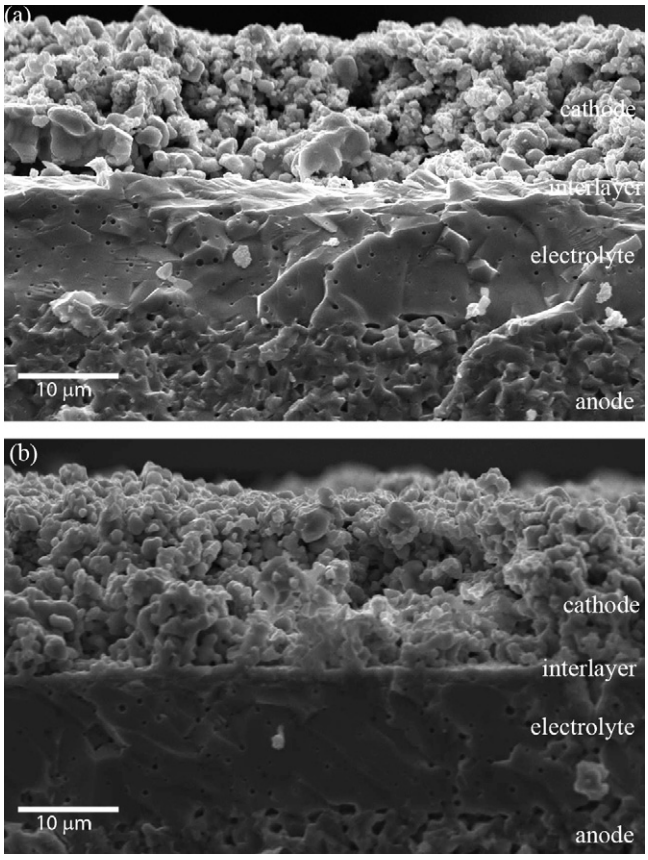

Fig. 8. SEM of the cell fabricated with the LSCF cathodes fired at (a) 1000 °C and (b) 1100 °C.

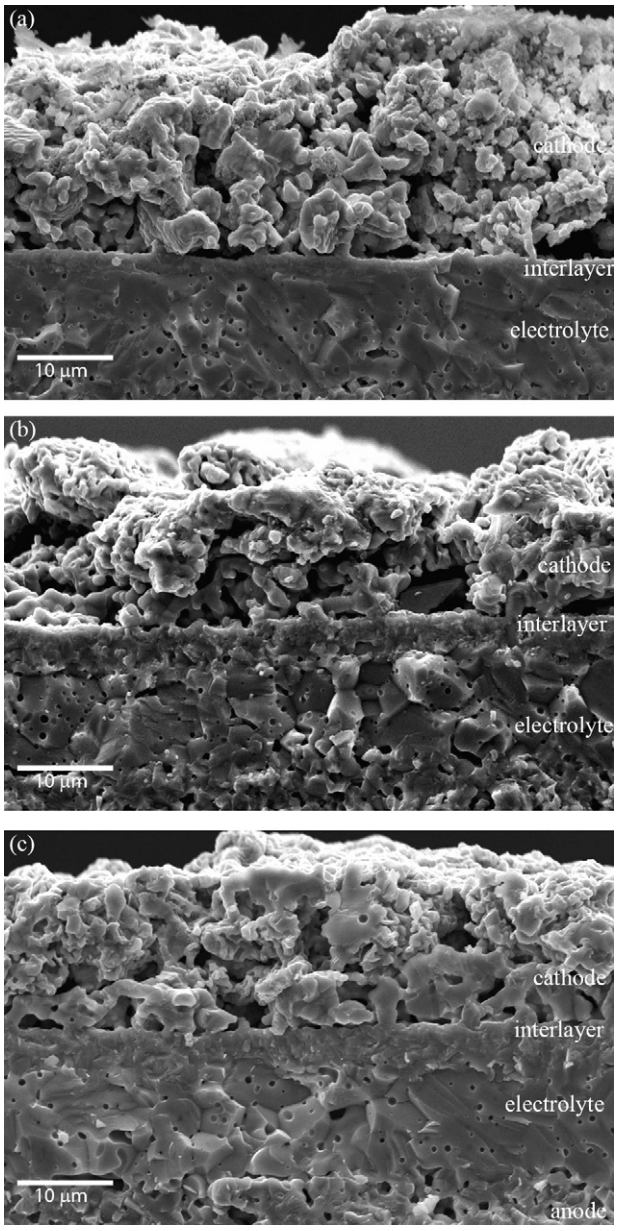

Fig. 9. SEM of the cell fabricated with (a) NSC, (b) NSCF, and (c) NSCF–Ag cathodes.

interlayer (<15 μm) and their ionic resistivities, the major contributor to this overpotential could be the electrical resistivity of the cathode. The fact that the magnitude of the slope of the *I–V* curves for the Fe-doped cathodes is greater than that for the undoped cathodes is clear evidence that the substitution of Fe for Co decreases the electrical conductivity of the cathode, resulting in a greater ohmic polarization at moderate current densities.

The poor performance of the NSCF-based cells sintered at 1200 °C relative to the LSCF-based cells sintered at 1100 °C and 1000 °C, even at low currents, suggests that the higher sintering temperature used to produce the NSCF-based cells may have resulted in densification of the cathode, thereby decreasing the number of reaction sites available for the oxygen reduction reaction and leading to activation polarization. The differences in the microstructures are also apparent on comparing the micrographs shown in Figs. 9b and 8b. This suggests that a lower sintering temperature for the NSCF-based cells may lead to improved performance.

4.4. Influence of the impregnation of NSCF with Ag

The poor performance of the Fe-doped cathodes relative to the undoped NSC and LSC cathodes suggests that improving the electrical conductivity of the cathode material could have a positive effect on cell performance. Accordingly, impregnation of the NSCF cathode was pursued with silver, which increases the electrical conductivity of the cathode by creating a continuous, conducting Ag phase. Fig. 9c is an SEM micrograph of the fracture surface of a cell fabricated with a NSCF–Ag cathode. This micrograph shows that the infiltration process does not adversely affect the pore structure in the cathode. Comparison of the performances of the cells fabricated with the NSCF and the NSCF–Ag cathodes (Fig. 5b and c) confirm that the presence of the conducting Ag increases the performance of the cell by reducing the activation polarization of the cathode. However, the performance of the NSCF-based cell impregnated with silver is still slightly below that of the undoped NSC-based cells. This demonstrates that although electrical conductivity is an important contributor to cell performance, other factors such as ionic conductivity and microstructure could also contribute to the cell performance.

5. Conclusions

Anode-supported, planar SOFC with thin YSZ electrolytes were successfully produced. Dense electrolytes bonded to porous anodes were prepared by tape casting and co-firing. Interlayers and cathodes were applied to the anode/electrolyte assemblies by screen printing and the membrane/electrode assemblies were then fired. The resulting cells exhibited adequate bonding and, utilizing low cathode firing temperatures, chemical reactions between the cell components were prevented. Electrochemical tests were conducted at temperatures of 600–800 °C.

The results show that the sintering temperature of the cathode plays an important role in determining the cell performance of the perovskite-based cathodes. Higher cathode sintering temperature results in a reduction in cell performance due to particle coarsening. The increase in the particle size and neck diameter during coarsening reduces the number of active reaction sites in the cathode. However, it is expected that very low sintering temperatures would also result in poor performance due to inferior conductivity resulting from insufficient connectivity between the particles and to the large fraction of pores. Thus, an optimum cathode sintering temperature must be determined for each cathode composition.

These results show that the performance of cells made with the NSC cathodes were comparable to those of cells produced with the LSC cathodes, while offering a reduction in TEC mismatch with the YSZ electrolyte. The lower TEC mismatch is expected to result in reduced long-term degradation observed during thermal cycling of SOFC [20]. Although NSCF cathodes exhibit an even lower TEC mismatch with YSZ compared to the NSC cathode, its performance is inferior. However, impregnation of the NSCF cathodes with silver increases the electrical conductivity of the cathode and improves the cell performance significantly, while still maintaining a low TEC mismatch with YSZ. This strategy may prove to be an effective mean of balancing the short-term performance that comes with cathodes having high electrical conductivity against the long term durability that comes with cathodes having lower TEC.

Acknowledgment

Financial support by the Welch Foundation grant F-1254 is gratefully acknowledged.

References

[1] S.A. Barnett, Energy 15 (1990) 1–9.
[2] K. Krist, J.D. Wright, in: S.C. Singhal, H. Iwahara (Eds.), Third International Symposium on Solid Oxide Fuel Cells, vol. PV 93–4, The Electrochemical Society, Inc, Honolulu, HI, 1993, pp. 782–791.
[3] F. Tietz, H.P. Buchkremer, D. Stöver, Solid State Ionics 152–153 (2002) 373–381.
[4] J. Will, A. Mitterdorfer, C. Kleinlogel, D. Perednis, L.J. Gauckler, Solid State Ionics 131 (2000) 79–96.
[5] J.A.M. Van Roosmalen, E.H.P. Cordfunke, Solid State Ionics 52 (1992) 303–312.
[6] A. Hammouche, E. Siebert, A. Hammou, Mater. Res. Bull. 24 (1989) 367–380.
[7] R.A. De Souza, J.A. Kliner, Solid State Ionics 106 (1998) 175–187.
[8] S.J. Skinner, Int. J. Inorg. Mater. 3 (2001) 113–121.
[9] H. Yokokawa, T. Horita, in: S.C. Singhal, K. Kendall (Eds.), High Temperature Solid Oxide Fuel Cells: Fundamentals, Design and Applications, Elsevier Advanced Technology, Oxford, UK, 2003.
[10] S.B. Adler, Solid State Ionics 111 (1998) 125–134.
[11] S.P.S. Badwal, S.P. Jiang, J. Love, J. Nowotny, M. Rekas, E.R. Vance, Ceram. Int. 27 (2001) 419–429.
[12] A. Petric, P. Huang, F. Tietz, Solid State Ionics 135 (2000) 719–725.
[13] Y. Sakaki, Y. Takeda, A. Kato, N. Imanishi, O. Yamamoto, M. Hattori, M. Iio, Y. Esaki, Solid State Ionics 118 (1999) 187–194.
[14] H.Y. Tu, Y. Takeda, N. Imanishi, O. Yamamoto, Solid State Ionics 117 (1999) 277–281.
[15] K.T. Lee, A. Manthiram, J. Electrochem. Soc. 153 (2006) A794–A798.
[16] K.T. Lee, A. Manthiram, J. Electrochem. Soc. 152 (2005) A197–A204.
[17] K.T. Lee, A. Manthiram, Solid State Ionics 176 (2005) 1521–1527.
[18] K.T. Lee, A. Manthiram, J. Power Sources 160 (2006) 903–908.
[19] L.A. Chick, L.R. Pederson, G.D. Maupin, J.L. Bates, L.E. Thomas, G.J. Exarhos, Mater. Lett. 10 (1990) 6–12.
[20] N.Q. Minh, J. Am. Ceram. Soc. 76 (1993) 563–588.
[21] A. Mukherjee, B. Maiti, A. Das Sharma, R.N. Basu, H.S. Maiti, Ceram. Int. 27 (2001) 731–739.
[22] R.E. Mistler, E.R. Twiname, Tape Casting: theory and practice, The American Ceramic Society, Westerville, OH, 2000, p. 298.